Cylindrical Couette Flows in the Transition Regime by the Method of Moments

Xiao-Jun GU*, David R. Emerson

* Corresponding author: Tel.: ++44 (0)1925 603664; Fax: ++44 (0)1925 603634;
Email: xiaojun.gu@stfc.ac.uk
Scientific Computing Department, STFC Daresbury Laboratory, Warrington, WA4 4AD, UK

Abstract The moment method is employed to study the characteristics of cylindrical Couette gas flow under rarefied conditions. Computed velocity profiles from the linearised R13 and R26 moment equations are compared with direct simulation Monte Carlo data. It is found that the moment method can extend the macroscopic equations into the early transition regime, but the surface curvature narrows the validity range of the macroscopic models. The slip velocity on the inner and outer cylinder is not equal due to curvature effects and the torque acting on the cylinder wall decreases as the rarefaction becomes stronger.

Keywords: Moment method, Cylindrical Couette, Knudsen Number, Rarefied Gas

1. Introduction

Gas flows in micro-electro-mechanical systems (MEMS) suffer from rarefied effects since the gas molecules collide with solid walls more often than among themselves to reach to the equilibrium state. As a result, the traditional hydro-thermal-dynamic model, the Navier-Stokes-Fourier (NSF) equations, fail to capture many nonequilibrium phenomena associated with rarefaction. The extent of the rarefaction is measured by the Knudsen number, Kn, the ratio of the molecular mean free path, λ, to the characteristic length of the geometry. When $Kn < 0.1$, i.e. in the slip-flow regime, the NSF equations coupled with appropriate velocity-slip and temperature-jump wall boundary conditions may predict certain main features of the flow. When the Knudsen number is greater than 0.1, in the transition regime, usually kinetic theory is required to study the flow details. The Boltzmann equation (Cercignani 1988) and direct simulation Monte Carlo (DSMC) (Bird, 1994) are the main kinetic methods to simulate nonequilibrium gas flow. However, they are computationally expensive, particularly for flows at low speed in the early transition regime. Despite significant effort being made to overcome the numerical difficulties and computing costs, solutions using the Boltzmann equation or DSMC are still too difficult to be widely used in practical engineering applications. Alternative approaches have been developed to alleviate the difficulties in kinetic theory and are accurate enough for engineering design.

Extending hydro-thermal-dynamics into the transition regime is one of the most promising approaches (Struchtrup 2005). The method of moments, which was originally proposed by Grad (1949) as an approximate solution procedure to the Boltzmann equation, is currently being used to bridge the gap between hydro-thermal-dynamics and kinetic theory. In this approach, the Boltzmann equation is satisfied in a certain average sense rather than at the molecular distribution function level. How far the hydro-thermal-dynamics should be extended, i.e. how many moments should be used, largely depend on the flow regime. It was found (Young 2011; Gu et al. 2010) that the regularized 13 moment equations (R13) are not adequate enough to capture the Knudsen layer in Kramers' problem and the regularised 26 moment equations (R26) are required to accurately reproduce the velocity defect found with kinetic data. However, both the R13 and R26 equation models can capture many nonequilibrium phenomena produced by

kinetic theory, such as the tangential heat flux in planar Couette flow and the bimodal temperature profile in planar force-driven Poiseuille flow in the early transition regime with different accuracy (Gu and Emerson 2009, 2011; Taheri et al. 2009; Struchtrup and Taheri 2011). In the present study, we investigate the effect of streamline curvature on the accuracy of the results obtained by the moment method.

One of the simplest situations involving curvature is the problem of shear flow between two concentric, rotating cylinders of infinite length, i.e. cylindrical Couette flow. It has been studied by various methods in different regimes (Cercignani and Sernagiotto 1967; Stefanov and Cercignani 1993; Tibbs et al. 1997, Aoki et al. 2003; Yuhong et al. 2005; Taheri and Struchtrup 2009). For many low speed flows, it should be sufficient to use a linearised set of moment equations. In the present study, both the linearised R13 (LR13) and R26 (LR26) equations are used to study the behaviour of cylindrical Couette flow in the early transition regime. The predicted results from the moment equations are compared with kinetic data for a range of Knudsen number, which is defined as the ratio of the mean free path to the gap between the two cylinders. In addition, the curvature effect on the velocity and shear stress are analysed in the present study.

2. Linearised Moment Equations and Wall Boundary Conditions for Cylindrical Couette Flows

The derivation of the R13 and R26 moment equations for a monatomic gas of Maxwell molecules and their linearisation can be found in Refs (Struchtrup and Torrilhon 2003; Gu and Emerson 2008; Taheri et al. 2009; Gu et al. 2009), respectively. In addition to the traditional thermo-hydro-dynamic variables, the pressure, p, (the density, ρ), the temperature, T, and the velocity, u_i, to describe the flows with the conservation laws, the R13 method adopts the governing equations for the stress σ_{ij} and the heat flux, q_i to account for the nonequilibrium effects. In the frame of the R26 method, it includes the higher moments of the molecular distribution function, m_{ijk}, R_{ij} and Δ in the governing equations.

For isothermal monatomic gas confined in two coaxial cylinders with infinite length, the cylindrical coordinates, $x_i = \{r, \theta, z\}$, are employed, where r is the radial coordinate, θ the azimuth and z the length coordinate. With the symmetry of the geometry and flow, the LR26 moment equations can be expressed in one dimensional form as:

$$\frac{\partial \bar{\sigma}_{r\theta}}{\partial \bar{r}} + 2\frac{\bar{\sigma}_{r\theta}}{\bar{r}} = 0, \tag{1}$$

$$\frac{\partial \bar{r}\bar{m}_{rr\theta}}{\bar{r}\partial \bar{r}} + \frac{\bar{m}_{rr\theta}}{\bar{r}} - \frac{\bar{m}_{\theta\theta\theta}}{\bar{r}} = -\sqrt{\frac{\pi}{2}}\bar{\sigma}_{r\theta} - \bar{r}\frac{\partial}{\partial r}\left(\frac{\bar{u}}{\bar{r}}\right) - \frac{2}{5}\bar{r}\frac{\partial}{\partial \bar{r}}\left(\frac{\bar{q}_\theta}{\bar{r}}\right), \tag{2}$$

$$\frac{\partial \bar{r}\bar{R}_{r\theta}}{\bar{r}\partial \bar{r}} + \frac{\bar{R}_{r\theta}}{\bar{r}} = -\frac{4}{3}\sqrt{\frac{\pi}{2}}\bar{q}_\theta - 2\left(\frac{\partial \bar{\sigma}_{r\theta}}{\partial \bar{r}} + 2\frac{\bar{\sigma}_{r\theta}}{\bar{r}}\right), \tag{3}$$

$$\frac{\partial \bar{r}\bar{\phi}_{rrr\theta}}{\bar{r}\partial \bar{r}} + \frac{\bar{\phi}_{rrr\theta}}{\bar{r}} - 2\frac{\bar{\phi}_{r\theta\theta\theta}}{\bar{r}} = -\frac{3}{2}\sqrt{\frac{\pi}{2}}\bar{m}_{rr\theta} - \frac{2}{5}\left(4\frac{\partial \bar{\sigma}_{r\theta}}{\partial \bar{r}} - 7\frac{\bar{\sigma}_{r\theta}}{\bar{r}}\right) - \frac{2}{35}\left(4\frac{\partial \bar{R}_{r\theta}}{\partial \bar{r}} - 7\frac{\bar{R}_{r\theta}}{\bar{r}}\right), \tag{4}$$

$$\frac{\partial \bar{r}\bar{\phi}_{r\theta\theta\theta}}{\bar{r}\partial \bar{r}} + 3\frac{\bar{\phi}_{r\theta\theta\theta}}{\bar{r}} = -\frac{3}{2}\sqrt{\frac{\pi}{2}}\bar{m}_{\theta\theta\theta} - \frac{6}{5}\left(3\frac{\bar{\sigma}_{r\theta}}{\bar{r}} - \frac{\partial \bar{\sigma}_{r\theta}}{\partial \bar{r}}\right) - \frac{6}{35}\left(3\frac{\bar{R}_{r\theta}}{\bar{r}} - \frac{\partial \bar{R}_{r\theta}}{\partial \bar{r}}\right), \tag{5}$$

$$\frac{\partial \bar{r}\bar{\psi}_{rr\theta}}{\bar{r}\partial \bar{r}} + \frac{\bar{\psi}_{rr\theta}}{\bar{r}} - \frac{\bar{\psi}_{\theta\theta\theta}}{\bar{r}} = -\frac{7}{6}\sqrt{\frac{\pi}{2}}\bar{R}_{r\theta} - \frac{14}{5}\left(\frac{\partial \bar{q}_\theta}{\partial \bar{r}} - \frac{\bar{q}_\theta}{\bar{r}}\right) - \frac{1}{5}\left(\frac{\partial \bar{\Omega}_\theta}{\partial \bar{r}} - \frac{\bar{\Omega}_\theta}{\bar{r}}\right) - 2\left(\frac{\partial \bar{m}_{rr\theta}}{\partial \bar{r}} + 2\frac{\bar{m}_{rr\theta}}{\bar{r}} - \frac{\bar{m}_{\theta\theta\theta}}{\bar{r}}\right), \tag{6}$$

which are closed by the following approximations:

$$\bar{\phi}_{rrr\theta} = -\frac{3}{7Z}\sqrt{\frac{2}{\pi}}\left(5\frac{\partial \bar{m}_{rr\theta}}{\partial \bar{r}} + \frac{2\bar{m}_{\theta\theta\theta} - 11\bar{m}_{rr\theta}}{\bar{r}}\right), \tag{7}$$

$$\bar{\phi}_{r\theta\theta\theta} = -\frac{1}{Z}\sqrt{\frac{2}{\pi}}\left[\frac{\partial \bar{m}_{\theta\theta\theta}}{\partial \bar{r}} - \frac{6}{7}\frac{\partial \bar{m}_{rr\theta}}{\partial \bar{r}} + \frac{15}{7}\left(\frac{2\bar{m}_{rr\theta} - \bar{m}_{\theta\theta\theta}}{\bar{r}}\right)\right], \tag{8}$$

$$\bar{\psi}_{rr\theta} = -\frac{18}{35Y}\sqrt{\frac{2}{\pi}}\left(4\frac{\partial \bar{R}_{r\theta}}{\partial \bar{r}} - 7\frac{\bar{R}_{r\theta}}{\bar{r}}\right), \tag{9}$$

$$\bar{\psi}_{\theta\theta\theta} = -\frac{54}{35Y}\sqrt{\frac{2}{\pi}}\left(3\frac{\bar{R}_{r\theta}}{\bar{r}} - \frac{\partial \bar{R}_{r\theta}}{\partial \bar{r}}\right), \tag{10}$$

$$\bar{\Omega}_{\theta} = -4\sqrt{\frac{2}{\pi}}\left(\frac{\partial \bar{R}_{r\theta}}{\partial \bar{r}} + 2\frac{\bar{R}_{r\theta}}{\bar{r}}\right), \tag{11}$$

in which, the collision constants Y = 1.698 and Z = 2.097 are Maxwell molecules (Gu and Emerson 2009).

The variables with an overbar symbol are small dimensionless deviations from the equilibrium state given by p_o, (or ρ_o), T_o and $u_{i,o}$ as defined by (Gu at al. 2009):

$$\begin{cases} u = (RT_o)^{1/2}\bar{u}, & \sigma_{r\theta} = \rho_o RT_o \bar{\sigma}_{r\theta}, \\ m_{rr\theta} = \rho_o (RT_o)^{\frac{3}{2}}\bar{m}_{rr\theta}, & m_{\theta\theta\theta} = \rho_o (RT_o)^{\frac{3}{2}}\bar{m}_{\theta\theta\theta}, \\ R_{r\theta} = \rho_o (RT_o)^{2}\bar{R}_{r\theta}, & q_{\theta} = \rho_o (RT_o)^{\frac{3}{2}}\bar{q}_{\theta}, \\ \psi_{rr\theta} = \rho_o (RT_o)^{\frac{5}{2}}\bar{\psi}_{rr\theta}, & \psi_{\theta\theta\theta} = \rho_o (RT_o)^{\frac{5}{2}}\bar{\psi}_{\theta\theta\theta}, \\ \phi_{rrr\theta} = \rho_o (RT_o)^{2}\bar{\phi}_{rrr\theta}, & \phi_{r\theta\theta\theta} = \rho_o (RT_o)^{2}\bar{\phi}_{r\theta\theta\theta}, \\ \Omega_{\theta} = \rho_o (RT_o)^{5/2}\bar{\Omega}_{\theta}, & r = \bar{r}\lambda, \end{cases} \tag{12}$$

in which, u and q_θ are the tangential velocity and heat flux, respectively, and $\sigma_{r\theta}$ the shear stress. The rest of the variables are the components of the higher moments in cylindrical coordinates. The mean free path, λ, is defined by

$$\lambda = \frac{\mu}{p_o}\sqrt{\frac{\pi RT_o}{2}} \tag{13}$$

with μ the viscosity and R the gas constant and the Knudsen number is $Kn = \lambda / L$. The characteristic length $L(= R_2 - R_1)$ is chosen to be the gap between the two cylinders with R_1 and R_2 the radius of the inner and outer cylinder wall, respectively.

The linearised Maxwell wall boundary conditions for the above equation set are (Gu et al. 2009):

$$\bar{u}_{\tau} = -G\bar{\sigma}_{r\theta} - \frac{5\bar{m}_{rr\theta} + 2\bar{q}_{\theta}}{10} + \frac{9\bar{\Omega}_{\theta} + 70\bar{\psi}_{rr\theta}}{2520}, \tag{14}$$

$$\bar{q}_{\theta} = -\frac{5G}{18}\left(7\bar{\sigma}_{r\theta} + \bar{R}_{r\theta}\right) - \frac{5\bar{u}_{\tau}}{3} - \frac{10\bar{m}_{nn\tau}}{9} - \frac{5\bar{\psi}_{nn\tau}}{81} - \frac{\bar{\Omega}_{\tau}}{56}, \tag{15}$$

$$\bar{m}_{rr\theta} = -G\left(\bar{\sigma}_{r\theta} + \frac{\bar{R}_{r\theta}}{7} + \frac{\bar{\phi}_{rrr\theta}}{3}\right) - \frac{2}{5}\bar{q}_{\theta} - \frac{2\bar{u}_{\tau}}{3} - \frac{\bar{\psi}_{rr\theta}}{18} - \frac{\bar{\Omega}_{\theta}}{140} \tag{16}$$

$$\bar{m}_{\theta\theta\theta} = -G\left(3\bar{\sigma}_{r\theta} + \frac{3\bar{R}_{r\theta}}{7} + \bar{\phi}_{r\theta\theta\theta}\right) - 3\bar{u}_{\tau} - \frac{3\bar{m}_{rr\theta}}{2} - \frac{9\bar{q}_{\theta}}{5} - \frac{9\bar{\Omega}_{\theta}}{280} - \frac{\bar{\psi}_{\theta\theta\theta}}{18} - \frac{\bar{\psi}_{rr\theta}}{12}, \tag{17}$$

in which, $\bar{u}_{\tau}$ is slip velocity of the gas on the wall. Here $G = \sqrt{\pi/2}(2-\alpha)/\alpha$ and α is the tangential momentum accommodation coefficient, indicating that a fraction, α, of gas molecules will be diffusely reflected with a Maxwellian at the wall temperature and the remaining fraction will undergo specular reflection. The accommodation coefficient, α, can have different values, α_1 and α_2, at the inner and outer wall, respectively. However, in the present study, we assume that both walls have the same properties so that $\alpha = \alpha_1 = \alpha_2$.

3. Results of Linearised Moment Equations in Comparison with Kinetic Theory

The LR26 moment equations can be reduced to a system of six moments for isothermal cylindrical Couette. Although analytical solutions have been obtained from the LR13 (Taheri and Struchtrup 2009) and NSF (Yuhong et al. 2005) equations, it is non-trivial to obtain an analytical solution from the LR26 equations for cylindrical Couette flow. However, it is convenient to solve them numerically, as they are one-dimensional linear differential equations. In the present

study, all of the three macroscopic models are solved numerically and a first-order slip boundary condition is used in association with the NSF equations.

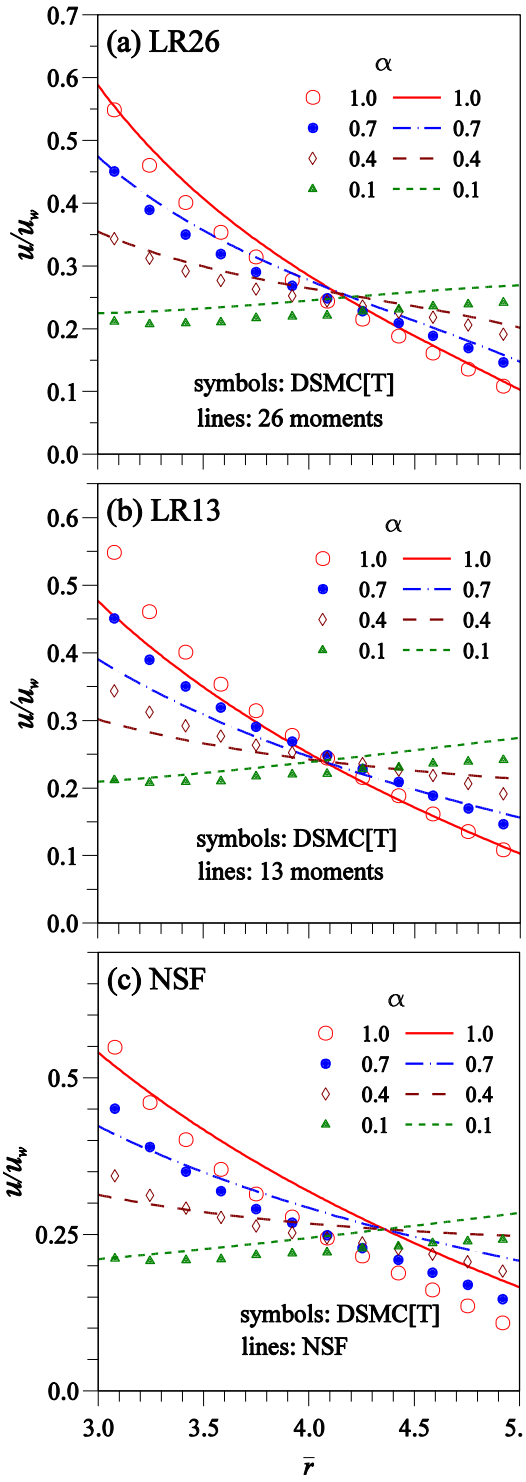

Fig. 1. Angular gas velocity against radial distance of the cylindrical Couette flow at Kn=0.5 and different α.. Inner cylinder with a wall velocity u_w and outer cylinder stationary. Line curves: (a) LR26; (b) LR13; (c) NSF. Symbols: DSMC data (T: Tibbs et al. 1997).

3.1 Velocity profile

Tibbs et al. (1997) performed a number of DSMC simulations with R_1=3λ, R_2=5λ (i.e. Kn=0.5) and four values of accommodation coefficient, α. Aoki et al. (2003) conducted a series of DSMC simulations with R_2/R_1=2 and the Knudsen number from 0.02 to 100. Both of them set the outer cylinder as stationary and the inner cylinder rotating at a wall velocity, u_w. Only the velocity profile data of the DSMC simulation were presented in their studies, which are the database used in the present study to benchmark the accuracy of our macroscopic models.

Shown in Fig. 1 are the predictions of the macroscopic models in comparison with the DSMC data of Tibbs et al. (1997). The LR26 equations predict the velocity profiles with reasonable accuracy for the fully diffusive to the specular reflection dominated walls. Although the LR13 equations do not perform well close to the inner cylinder wall, they are fairly adequate close to the outer cylinder wall. It is interesting to note that the NSF equations perform better than the LR13 equations close to the inner cylinder wall but worse in the outer cylinder region as indicated in Figs. 1(b) and (c).

The accuracy of the moment method is further checked at lower and higher values of Knudsen number. The line curves illustrated in Fig. 2 are the velocity profiles obtained from hydro-thermal-dynamic models of different sophistication at Kn = 0.1, 0.5 and 1 and the accommodation coefficient, α, at the cylinder walls is 1.0 and 0.05, respectively. The DSMC data are presented with symbols.

At Kn = 0.1, the upper limit of the slip regime, the predictions of the three models are close to each other and in a good agreement with the DSMC data. When both walls are fully diffusive at α = 1, the gas moves faster close to the inner wall than at the outer wall. As the walls change from the diffusive to near specular reflection at α = 0.05, the gas inside the gap of the cylinders moves almost at the same speed due to the curvature effect.

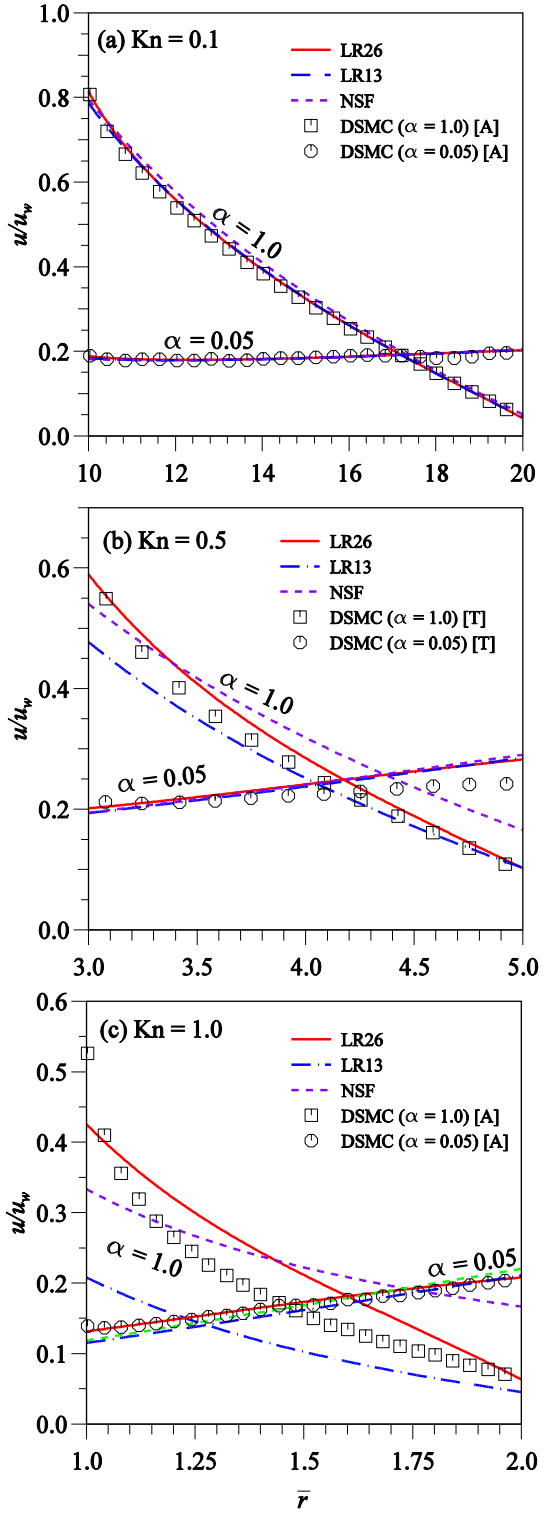

Fig. 2. Angular gas velocity against radial distance of the cylindrical Couette flow at different *Kn* and α. Inner cylinder with a wall velocity u_w and outer cylinder stationary. Line curves: macroscopic models. Symbols: DSMC data (A: Aoki *et al.* 2003; T: Tibbs et al. 1997).

As the flow enters into the transition regime, the discrepancy among the macroscopic models starts to appear. At *Kn* = 0.5 and α = 1 as shown Fig. 2(b), the LR26 equations can follow the DSMC data fairly accurately close to the walls and inside the gap between the two cylinders. The LR13 equations overpredict the slip velocity close to the inner wall whilst the NSF equations with a first order wall boundary condition overpredict the slip velocity close to the outer wall. Taheri and Struchtrup (2009) constructed a second order slip boundary condition by retaining some of the underlined terms in Eq. (14) and presented NSF results for velocity first and second order slip boundary condition. With the second order slip boundary condition, the NSF prediction shifts towards the LR13 solution. The discrepancy between the LR13 and the NSF equations with the second order boundary condition is not significant in terms of velocity profiles.

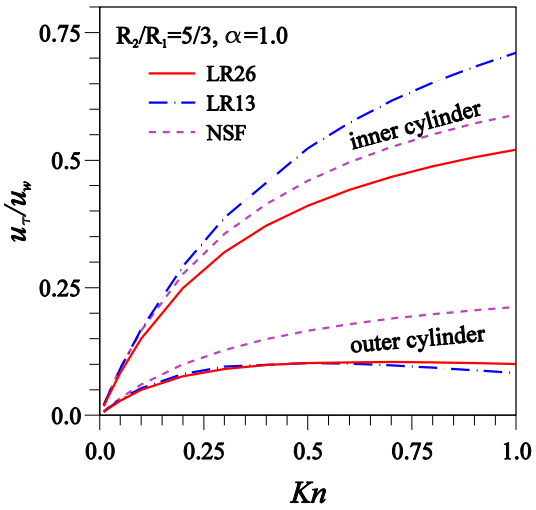

Fig. 3. Normalised slip velocity u_τ/u_w, on fully diffusive cylinder walls against the Knudsen number *Kn*. Inner cylinder with a wall velocity u_w and outer cylinder stationary.

Shown in Fig. 2(c) is the velocity profiles for *Kn* = 1. In this case, not only the Knudsen number is large, the curvature is also greater than those in Figs. 2 (a) and (b), as the radii of the cylinders are much smaller. None of the three macroscopic models can capture the velocity profile produced by the DSMC simulation for α = 1 adequately, although the prediction of the LR26 equations are much closer to the DSMC data than the LR13 and

NSF equations. When the curvature of the surface is large, in addition to the Knudsen layer in the planar surface, there is an S-layer on the convex surface (Sone 1973), which narrows the validity range of macroscopic models (Dinler et al. 2013). However, if the value of the accommodation coefficient is smaller than a critical value, velocity inversion occurs. All of three models reproduce this phenomena as demonstrated in Fig. 2 for α = 0.05.

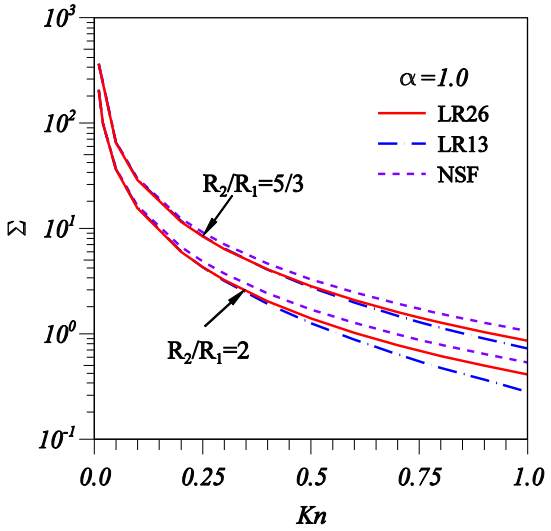

Fig. 4 Normalised torque on the cylinder wall of cylindrical Couette flow against the Knudsen number for α = 1.

3.2 Velocity slip

In planar Couette flows, the velocity slip on both walls is equal. In cylindrical Couette flows, the velocity slip, u_τ, on the inner and outer wall is different due to the curvature effect. In the case of R_2/R_1 = 5/3 and α = 1, the normalized slip velocity, u_τ/u_w, on both walls predicted by the macroscopic models are presented in Fig. 3. The slip velocity on the inner cylinder is greater than that on the other cylinder. The LR13 equations produce the largest slip velocity among the three macroscopic models while the LR26 equations the lowest. On the outer cylinder, the LR26 and LR13 equations predict similar values of velocity slip. The NSF equations with the first order wall boundary condition overpredict the velocity slip. The velocity slip on the inner cylinder becomes larger as the Knudsen number increases. The velocity slip on the outer cylinder, on the other hand, increases as the Knudsen number increases when Kn < 0.5 and slightly decreases when Kn > 0.5 from the moment method.

3.3 Shear stress and torque

In non-equilibrium planar Couette flow, the shear stress of the flow is a constant dependent on the Knudsen number and the wall condition (Sone et al. 1990). This is no longer the case in cylindrical Couette flow due to the curvature effect. From Eq. (1), the shear stress, $\bar{\sigma}_{r\theta}$, is readily obtained by

$$\bar{\sigma}_{r\theta} = \frac{A}{\bar{r}^2} \quad \text{or} \quad A = \bar{r}^2 \bar{\sigma}_{r\theta} \tag{18}$$

in which, A is a constant determined by the boundary conditions. In fact, the constant A represents the torque acting on the cylinder wall. Shown in Fig. 4 is the rescaled torque $\Sigma = A/\bar{u}_w$ predicted from the macroscopic models against the Knudsen number for R_2/R_1= 5/3 and 2, respectively. When Kn < 0.2, three models produce the values of torque close to each other. When Kn is greater than 0.2, the NSF equations give the larger value of torque than the moment equations. As the Knudsen number increases, the torque on the cylinder wall reduces dramatically. At the same Knudsen number, the larger the value of R_2/R_1, the smaller the torque.

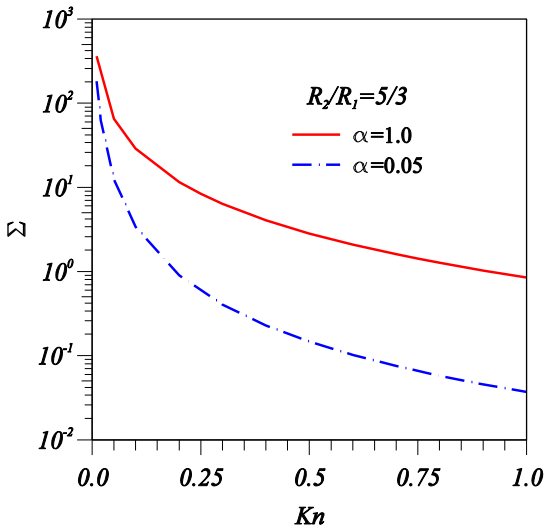

Fig. 5 Effect of accommodation coefficient on torque on the cylinder wall of cylindrical Couette flow against the Knudsen number.

The accommodation coefficient has a significant effect on the magnitude of the torque as indicated by the solution of the LR26 equations in Fig. 5 In comparison with fully diffusive walls, the torque on the specular dominated walls (α = 0.05) is much smaller from the LR26 equations for R_2/R_1=5/3, particularly at large Knudsen number.

4. Conclusions

The moment method is employed to study rarefaction effects on cylindrical Couette flow. In comparison with kinetic theory, the LR26 moment equations can be applied adequately up to *Kn* = 0.5 in a domain with curved surfaces. It was shown that the velocity-slip on the inner cylinder is greater than that on the outer cylinder due to curvature effects. The shear stress in cylindrical Couette flow is no longer a constant whilst the torque acting on the cylinder wall decreases as the rarefaction effect becomes stronger.

Acknowledgement

The authors would like to thank the Engineering and Physical Science Research Council (EPSRC) for their support of Collaborative Computational Project 12 (CCP12) and Programme grant (EP/I011927/1, Non-equilibrium fluid dynamics for Micro/Nano engineering systems)

References

Aoki, K., Yoshida, H., Nakanishi, T., Garcia. A.L., 2003. Inverted velocity profile in the cylindrical Couette flow of a rarefied gas. Phys. Rev. E 68, 016302.

Bird, G., 1994. Molecular Gas Dynamics and the Direct Simulation of Gas Flows. Clarendon Press, Oxford.

Cercignani, C., Sernagiotto, F., 1967. Cylindrical Couette Flow of a Rarefied Gas. Phys. Fluids 10, 1200-1204.

Cercignani, C., 1988. The Boltzmann Equation and Its Applications. Springer, New York.

Dinler, A., Barber, R.W., Emerson, D.R., Stefanov, S.K., Orucoglu, K., 2013. The effects of the S-layer on nonplanar microflows: A critical view on the accuracy of slip models. J. Comput. Theo. Nanosci. 10, 1990-1998.

Grad, H., 1949. On the kinetic theory of rarefied gases. Comm. Pure Appl. Math. 2, 331-407.

Gu, X.J., Emerson, D.R., 2009. A higher-order moment approach for capturing non-equilibrium phenomena in the transition regime. J. Fluids Mech. 636, 117-216.

Gu, X.J., Emerson, D.R., Tang, G.H., 2009. Kramers' problem and the Knudsen minimum: a theoretical analysis using a linearized 26-moment approach. Contin. Mech. Thermodyn., 21, 345-360.

Gu, X.J., Emerson, D.R., Tang, G.H., 2010. Analysis of the slip coefficient and defect velocity in the Knudsen layer of a rarefied gas using the linearized moment equations. Phys. Rev. E 81, 016313.

Gu, X.J., Emerson, D.R., 2011. Modeling oscillatory flows in the transition regime using a high-order moment method. Microfluid Nanofluid, 10, 389-401.

Sone, Y., 1973. New kind of boundary layer over a convex solid boundary in a rarefied gas. Phys. Fluids 16, 1422-1424.

Sone, Y., Takata, S., Ohwada, T., 1990. Numerical analysis of the plane Couette flow of a rarefied gas on the basis of the linearized Boltzmann equation for hard-sphere molecules. Eur. J. Mech., B/Fluids, 9, 273-288.

Stefanov, S., Cercignani, C., 1993. Monte Carlo simulation of the Taylor–Couette flow of a rarefied gas. J. Fluid Mech. 256, 199-213.

Struchtrup, H., Torrilhon, M., 2003. Regularisation of Grad's 13 moment equations: Derivation and linear analysis, Phys. Fluids, 15, 2668-2680.

Struchtrup, H., 2005. Macroscopic Transport Equations for Rarefied Gas Flows. Springer, Berlin.

Struchtrup, H., Taheri, P., 2011. Macroscopic transport models for rarefied gas flows: a brief review. IMA J. Appl. Math. 76, 672-697.

Taheri, P., Struchtrup, H., 2009. Effects of rarefaction in microflows between coaxial cylinders. Phys. Rev. E 80, 066317.

Taheri, P., Torrilhon, M., Struchtrup, H., 2009. Couette and Poiseuille microflows: Analytical solutions for regularized 13-moment equations. Phys. Fluids, 21, 017102.

Tibbs, K.W., Baras, F., Garcia A. L., 1997. Anomalous flow profile due to the curvature on slip length. Phys. Rev. E 56, 2282-2283.

Young, J.B., 2011. Calculation of Knudsen layers and jump conditions using the linearised G13 and R13 moment methods. Int. J. of Heat and Mass Transfer 54, 2902-2912.

Yuhong, S., Barber, R.W., Emerson, D.R., 2005. Inverted velocity profiles in rarefied cylindrical Couette gas flow and the impact of the accommodation coefficient. Phys Fluids 17, 047102.